Journal of Power Sources 244 (2013) 570–574

Contents lists available at SciVerse ScienceDirect

Journal of Power Sources

journal homepage: www.elsevier.com/locate/jpowsour

Short communication

Silicon/carbon nanocomposite pyrolyzed from phenolic resin as anode materials for lithium-ion batteries

Ming-Shan Wang, Li-Zhen Fan*

Institute of Advanced Materials and Technology, University of Science and Technology Beijing, Beijing 100083, China

HIGHLIGHTS

- Si/C nanocomposite is prepared by using phenolic resin as a carbon precursor.
- The Si particles are covered by a uniform nanosized carbon layer.
- Si/C nanocomposite exhibits higher electrochemical performance than bare Si and C.
- The capacity can be tuned by varying the ratio of Si to C.

ARTICLE INFO

Article history:
Received 15 October 2012
Received in revised form
17 January 2013
Accepted 26 January 2013
Available online 1 February 2013

Keywords:
Lithium-ion batteries
Silicon
Carbon
Nanocomposite
Anode

ABSTRACT

Silicon/carbon nanocomposite as anode materials for lithium-ion batteries is synthesized by a simple route using phenolic resin as a precursor. The Si nanoparticles with the size of 50–200 nm in diameter can be uniformly coated by carbon layer when the content of carbon is 58%. As an anode material for lithium-ion batteries, the Si/C nanocomposite exhibits a reversible capacity of 678 mAh g^{-1} after 50 cycles at a current density of 100 mA g^{-1}as well as excellent capacity retention at high rates. These improvements could be attributed to the introduction of carbon in the Si/C nanocomposite and carbon coatings on the surface of Si, which provide a rapid lithium transport pathway, reduce the cell impedance and stabilize the electrode structure during charge/discharge cycles.

1. Introduction

Silicon has been considered as a promising anode material for lithium-ion batteries due to its much higher specific capacity (4200 mAh g^{-1}) than the commercial graphite (372 mAh g^{-1}) [1]. Nevertheless, the most critical drawback of silicon-based anode is the large volume expansion–contraction during the lithium alloying–dealloying process, which eventually leads to the electrode pulverization and capacity fading [2–4]. To improve the electrochemical performance of silicon-based material, taking advantage of nanostructures is a popular method [5–7]. That is because of the following advantages: (1) a higher specific area could provide higher charge/discharge rates; (2) the accommodation of large volume change could improve the cycle life; (3) shorter lithium diffusion path could increase the power capabilities. Besides, the synthesis of novel nanostructured Si has also been done to improve the electrochemical stability of silicon-based anodes, such as porous Si [8], Si nanowires [9], nest-like silicon nanospheres [10]. Among those materials, dispersing silicon in a ductile carbon matrix, such as carbon coating [11–15], carbon nanotubes [16] and graphene [17], are also an attractive route to increase the cycling stability of silicon-based material. The carbon matrix can not only provide continuous long-distance electronic transport pathway, but also support numerous active sites for charge-transfer reactions. Furthermore, carbon matrix acted as a physical buffering layer could eliminate the large volume change. Besides, introducing inactive component, such as TiN [18], SiC [19], TiC [20], is also an approach to suppress the capacity fading and to retain the high capacity in anode composite materials for Li-ion batteries. The inactive component serves as a buffer matrix, which could decrease the irreversible capacity and improve the capacity retentions of the composite. In addition, many studies have also been focused on the advancement of the electrically

* Corresponding author. Tel./fax: +86 10 62334311.
E-mail addresses: fanlizhen@ustb.edu.cn, fanlizhen@gmail.com (L.-Z. Fan).

0378-7753/$ – see front matter © 2013 Elsevier B.V. All rights reserved.
http://dx.doi.org/10.1016/j.jpowsour.2013.01.151

inactive components of battery electrodes, such as binders [21,22]. It has been indicated that the stability and irreversible capacity of Si are great dependent on the binder's properties.

In this study, phenolic resin is selected as a carbon source because the pyrolyzed carbon exhibits the highly reversible capacity (about 400 mAh g^{-1}) and excellent cycling performance [23–25]. In addition, the first irreversible capacity could be optimized by optimizing the pyrolysis temperature. In order to combine the advantages of the high capacity of silicon and the good cycling behavior of carbon pyrolyzed from phenolic resin, the Si/C nanocomposite is synthesized by highly dispersing silicon nanoparticles in a gel of phenolic resin, followed by carbonization process under argon. This approach is simple and direct, and the as-prepared Si/C nanocomposite exhibits the satisfactory cycling stability and rate capability.

2. Experimental

Si/C nanocomposite was synthesized using the following procedure. Typically, 0.3 g phenolic resin was dissolved in 10 mL acetone under continuous stirring. 0.1 g Si with the particle size of 50–200 nm was then added into the above solution with ultrasonic stirring for 3 h. Along with ultrasonic stirring and drying at 40 °C, the acetone vaporized and solution was turned into orange gel. Then the dried substance was transferred into a furnace and pyrolyzed at 750 °C under argon atmosphere for 5 h. Finally, the Si/C nanocomposite was obtained after the temperature cooled down naturally to room temperature.

The crystal structure of the as-prepared nanocomposite was characterized by X-ray diffraction (XRD) with Cu Kα radiation (Rigaku D/max-RB)at 40 kV and 30 mA. Raman measurement was performed with a Horiba JobinYvon Raman spectrometer at the excitation wavelength of 514.4 nm. The thermogravimetric analysis was carried out by using a TGA/DSC1 type instrument (MettlerToledo, Switzerland) with a heating rate of 10 °C min^{-1} in air. The morphologies of the silicon and Si/C nanocomposite were observed using Field Emission Scanning Electron Microscope (FE-SEM, JSM-6330) and Transmission Electron Microscopy (TEM, JEM-2100F).

Electrochemical tests of the electrode materials were performed using half-cells with Si/C nanocomposite as a working electrode and lithium metal as a counter electrode. A 1 M $LiPF_6$ was dissolved in a 1:1:1(volume/volume/volume) mixture of ethylene carbonate, diethyl carbonate, and dimethyl carbonate as electrolyte and Celgard2400 membrane was used as separator. The working electrodes were prepared by mixing 60 wt% active materials (Si powder or nanocomposite), 20 wt% acetylene blank, and 20 wt% polyvinylidene fluoride dissolving in N-methyl-2-pyrrolidene solution. The cells were charged and discharged on a land test system (LAND CT2001A) in a voltage window of 0.01–1.5 V at 25 °C. Cyclic voltammetry (CV) and electrochemical impedance spectroscopy (EIS) were measured on an electrochemical workstation (CHI660C) at a scanning rate of 0.5 mV s^{-1}. EIS were recorded by applying an AC voltage of 10 mV amplitude over the frequency range from 10^5 to 0.01 Hz.

3. Results and discussion

Fig. 1 displays the typical XRD patterns of nanosized Si and Si/C nanocomposite. It is evident that the sharp peaks at $2\theta = 47°$, 56°, 69°, 76°, 87° reflect crystal Si with a cubic structure (JCPDS card No. 27-1402). After the carbon coating via carbonization process, the peak position and shape does not change significantly, indicating that the pyrolysis does not destroy the original crystalline structure. The diffraction peaks of Si/C nanocomposite also indicate a high purity of Si phase without other impurities after the pyrolysis Si/phenolic resin precursor. However, a broad hump is observed as shown at around $2\theta = 23°$ corresponding to the amorphous carbon in the Si/C nanocomposite.

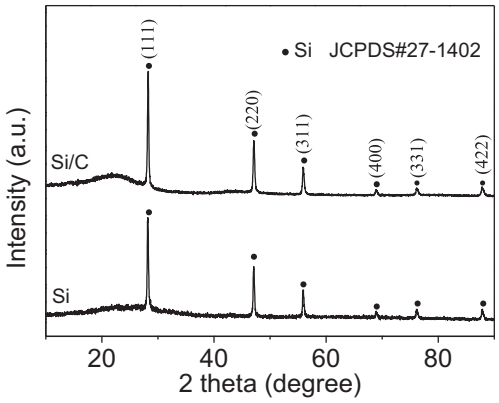

Fig. 1. XRD patterns of Si and Si/C nanocomposite.

The degree of graphitization of the carbon can be estimated from relative intensities of D band and G band in the Raman spectra (Fig. 2). The strong intense peak at 509 cm^{-1} is attributed to the Si–Si bending modes of Si. The silicon peak shifted after the coating of carbon, which is probably due to a phonon confinement effect or a masking effect [26]. The peaks at 1336 cm^{-1} and 1591 cm^{-1} correspond to D band and G band of graphite, which are related to the disorder-induced feature of carbon and graphitic crystallites of carbon materials, respectively [27]. The relatively ratios of intensity between D and G band is strong ($I_D/I_G = 0.93$) suggesting the low degree of graphitization of the Si/C nanocomposite.

The weight of carbon in Si/C nanocomposite can be calculated by TG curve. As shown in Fig. 3, the weight losses of Si/C nanocomposite occur in the temperature of 100–700 °C corresponding to the oxidation of the carbon. A little weight increase in the temperature over 700 °C is ascribed to the oxidation of silicon into SiO_x. When the temperature is higher than 700 °C, the carbon is completely combusted. Therefore, the weight of carbon in Si/C nanocomposite is estimated to be 58%.

The morphology of the Si and the as-prepared Si/C nanocomposite are characterized by FE-SEM and TEM. From Fig. 4a, it can be seen that the pristine silicon particles are connected and agglomerated heavily with the particle sizes of 50–200 nm. However, the Si/C nanocomposite displays the obvious difference from the pristine silicon (Fig. 4b). The particles distribute uniformly with the particle size around 150 nm, indicating that the agglomeration of nanoparticles is suppressed by continuing ultrasonic dispersion

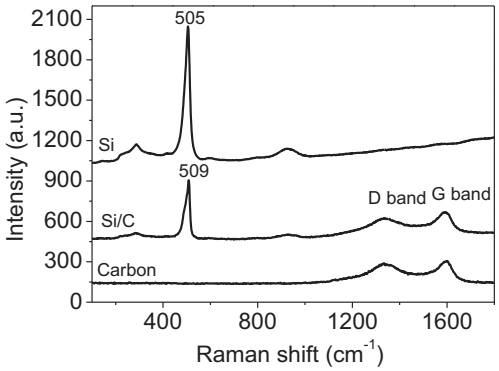

Fig. 2. Raman spectra of pyrolyzed carbon, Si, and Si/C nanocomposite.

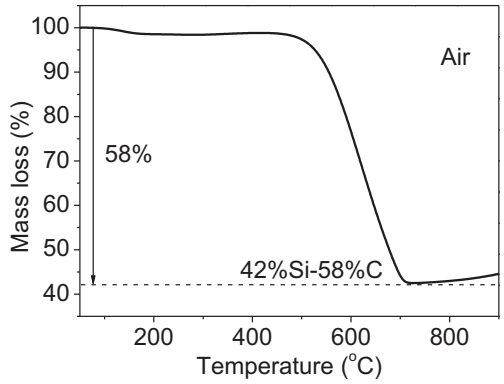

Fig. 3. TG curve of Si/C nanocomposite measured under air atmosphere.

during the gelatinizing process. In TEM image (Fig. 4c), it is evident that the Si particles are coated with a layer of carbon completely, preventing the particles from agglomeration. From high resolution TEM (Fig. 4d), it can be seen that the silicon particle is covered with a compact carbon layer. As shown in the SAED image of Fig. 4d inset, only a spot pattern is appeared in the core, which corresponds well to the (111), (220) and (311) planes of crystalline silicon.

Fig. 5 exhibits the CV curves of Si and Si/C nanocomposite at the scan rate of 0.5 mV s^{-1} in the range of 0.01–1.5 V. For both Si and Si/C nanocomposite, in the first cathodic scan, a distinctive reduction peak is observed at 0–0.2 V which is ascribed to the lithiation of silicon from a crystalline to an amorphous phase [28]. An irreversible cathodic peak is also seen at 0.5–0.75 V, which can be attributed to the formation of solid electrolyte interphase (SEI) film on the electrode surface [13,29], as this peak disappears in the subsequent cycles. For Si nanoparticles, in the first anodic scan, two peaks located at ~0.32 V and ~0.54 V are observed which are related to the dealloying of the Li–Si alloys [30]. For the Si/C nanocomposite, an anodic peak shown at ~0.25 V indicates that most of silicon turns into an amorphous Li_xSi phase [31]. It can also

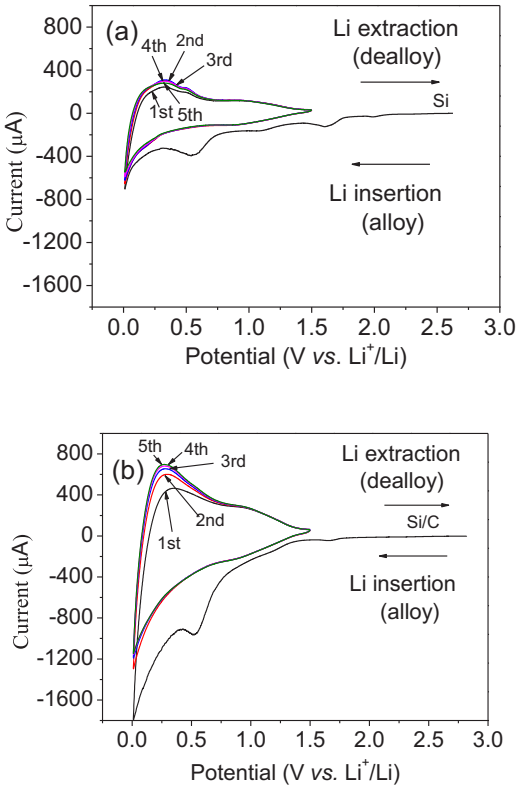

Fig. 5. CV curves of the first five cycles of the Si nanoparticles electrode (a) and the Si/C nanocomposite electrode (b) in the potential window between 0.01 and 1.5 V at a scan rate of 0.5 mV s^{-1}.

be seen that the current peaks of Si/C nanocomposite are much larger than those of the Si nanoparticle, indicating the migration of lithium ion into silicon host of Si/C nanocomposite is significantly larger than that of Si electrode.

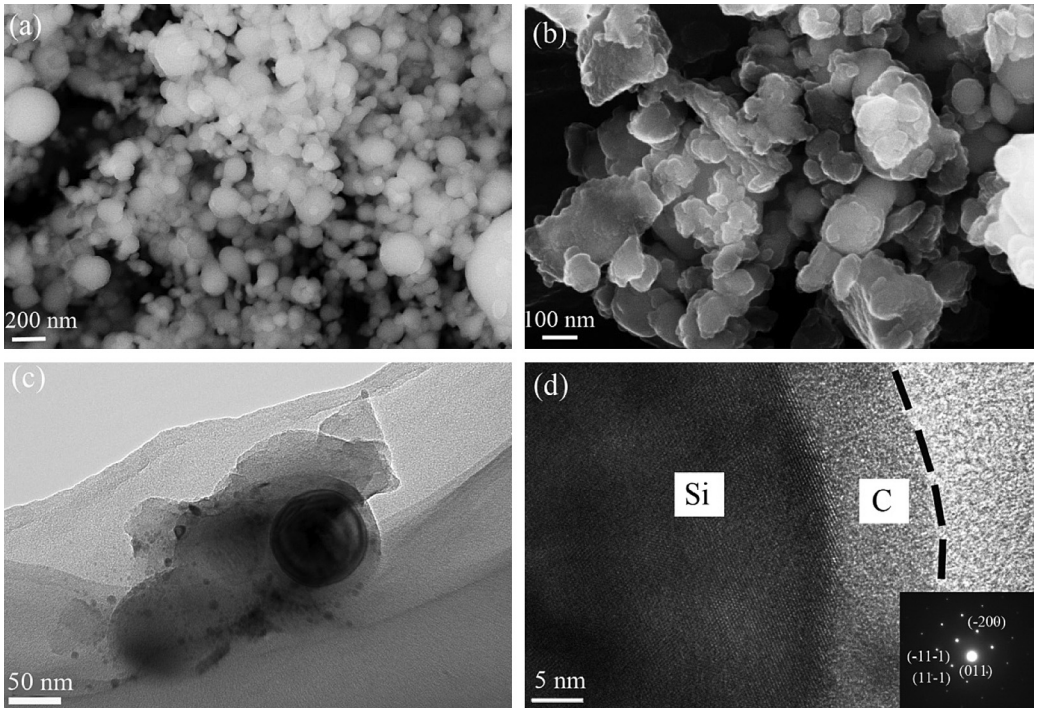

Fig. 4. FE-SEM images of Si (a) and Si/C nanocomposite (b); TEM images of Si/C nanocomposite (c, d), inset in (d) is the SAED image of Si.

Fig. 6a–c provide the voltage profiles of Si, Si/C and C electrodes for the 1st, 2nd, 5th, 10th, and 50th cycles at 100 mA g^{-1}between 0.01 V and 1.5 V. The first charge (Li insertion) and discharge (Li extraction) capacities of Si electrode are 3036 and 1737 mAh g^{-1}, with the irreversible capacity of 1300 mAh g^{-1}(Fig. 6a). The huge irreversible capacity of Si is ascribed to the formation of SEI film on the surface of silicon electrode [32,33]. A rapid capacity loss is observed for Si electrode and only 230 mAh $g^{-1}$is retained after 50 cycles (Fig. 6d). It is attributed to the poor electrical contact of Si electrode from the current collector resulting from the large volume change during the repeat cycles. For comparison, the Si/C nanocomposite (Fig. 6b) exhibited a first discharge capacity of 902 mAh g^{-1} (for Si/C composite, the capacity is calculated based on the total weight of the Si and carbon)with the columbic efficiency of 57%. The results mainly due to the large irreversible capacity of amorphous carbon (the initial columbic efficiency is 43%, as shown in Fig. 6c). After 10 cycles, the discharge capacity of Si/C nanocomposite increased to 960 mAh g^{-1}, indicating that the electrochemical activity of silicon increased during cycling. The columbic efficiency increase to above 97% after a few cycles. After 50 cycles, the discharge capacity of Si/C nanocomposite is 678 mAh g^{-1} (Fig. 6d), corresponding to 75% of the discharge capacity at the first cycle, which is much higher than those of bare Si electrode and C electrode. The better cycling performance of Si/C nanocomposite could be attributed to small Si nanoparticles and the synergistic effect of the Si/C composite.

The rate capabilities of Si and Si/C nanocomposite are further compared in Fig. 7. At the lower current density of 0.1 A g^{-1}, 0.2 A g^{-1}, and 0.5 A g^{-1}, the reversible capacities of Si/C nanocomposite are 900, 884, and 813 mAh g^{-1} respectively, which are much higher than that of Si at every current density. It also delivers high discharge capacity of 557 mAh g^{-1} and 465 mAh g^{-1} even at 3 A g^{-1} and 5 A g^{-1}, respectively. When the current density returns to 0.1 A g^{-1}, 105% of the initial capacity is delivered. The excellent cycle stability and rate capability of Si/C nanocomposite maybe attributed to the following reasons. Firstly, Si nanoparticles are completely coated by the disordered carbon layer, and more stable SEI film could be formed at the surface of Si/C electrode. As a result, the integrality of particles is retained during the charge/discharge process. Secondly, the carbon in the composite is beneficial to the transportation and diffusion of lithium ion. Thirdly, the suitable carbon can not only improve the electrical conductivity of the nanocomposite, but also decrease the inner resistance.

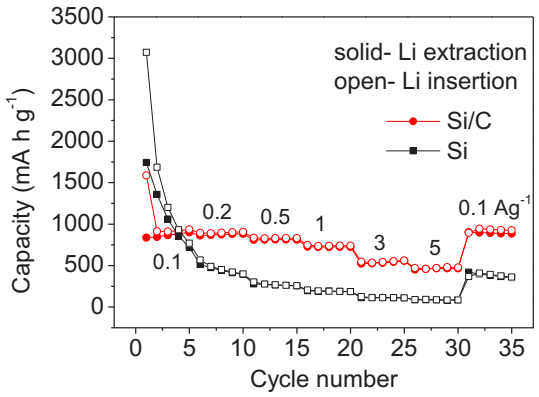

Fig. 7. Rate capability of the Si nanoparticles, pyrolyzed carbon, and Si/C nanocomposite in the potential window between 0.01 and1.5 V.

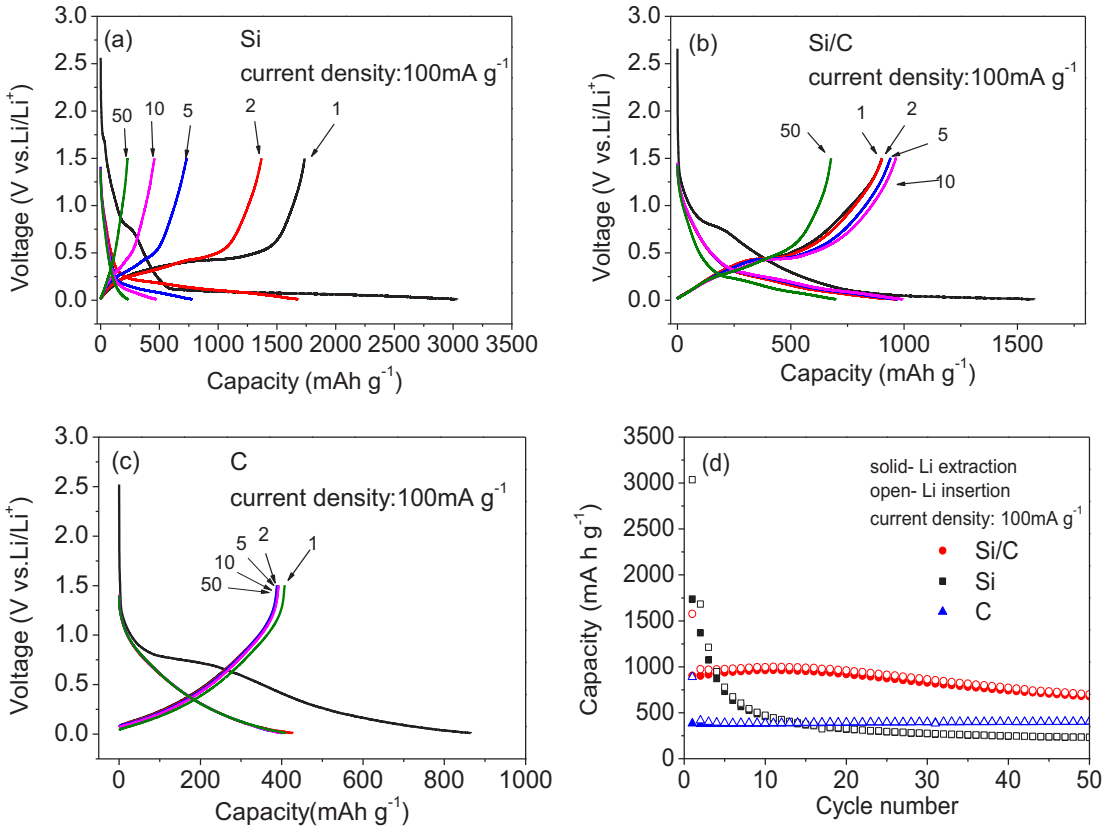

Fig. 6. Voltage profiles of (a) the Si nanoparticles electrode, (b) the Si/C nanocomposite electrode, (c) pyrolyzed carbon electrode after 1, 2, 5, 10, 50 cycles and (d) cycle stability of the Si nanoparticles, pyrolyzed carbon, and Si/C nanocomposite in the potential window between 0.01 and1.5 V.

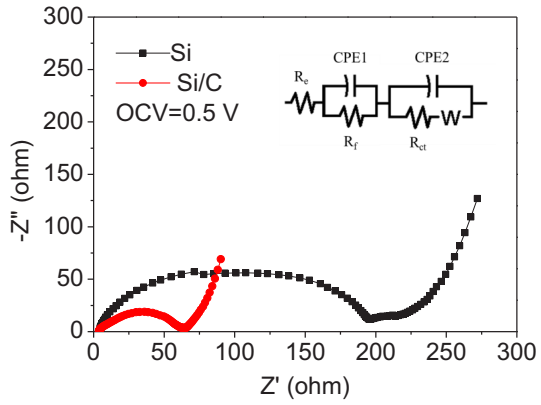

Fig. 8. Nyquist plots of Si nanoparticles and Si/C nanocomposite electrodes after 20 cycles at the discharged state, inset is the equivalent circuit used to describe the Li^+ insertion/extraction process.

Table 1
Equivalent circuit parameters obtained from fitting the experimental impedance spectra.

Sample	R_e (Ω)	R_f (Ω)	R_{ct} (Ω)	CPE1 (F)	CPE2 (F)	W (Ω $s^{-1/2}$)
Si	5.1	65.8	121.5	7.3E−7	4.6E−6	0.02
Si/C	4.1	10.1	43.1	2.7E−6	1.3E−5	0.06

Fig. 8 compares the Nyquist plots of Si and Si/C nanocomposite after five cycles at discharged state. As revealed in Fig. 8, both electrodes comprise one depressed semicircle in the high frequency range followed by a straight line portion in the low frequency range [34,35]. The diameter of the depressed semicircle represents the overlap between the resistance of SEI film and the charge-transfer resistance, while the straight line corresponds to the diffusion of lithium ion [36,37]. The modified equivalent circuit (Fig. 8 inset) is successfully used and the kinetic parameters are obtained by simulation. The fitting impedance data of the EIS for Si and Si/C composites are shown in Table 1, including the resistance for lithium ion transport in an electrolyte (R_e), surface film capacitance (CPE1) and the resistance for Li^+ migration through the surface film (R_f), charge-transfer resistance at the electrode and electrolyte interface (R_{ct}), double-layer capacitance (CPE2), and the Warburg impedance (W) that is related to the diffusion of lithium ions in solid electrode materials. The resistance change of R_e is similar for both Si and Si/C composite. Compared to the pure Si electrode, the decrease of R_f in Si/C is observed. That is because that a stable SEI film is formed after carbon coating, which decreases the resistance for Li^+ migration through the surface film. In addition, the smaller R_{ct} is also observed in Si/C composite, which means a smaller electrochemical reaction resistance due to the electronic contact loss during the lithiation/delithiation process for Si/C electrode. It also indicates that the carbon layer supplies fast charge-transfer channels on the interface of Si and electrolyte. As seen from Table 1, the values of CPE1 are less than those of CPE2 in both Si and Si/C electrodes, which indicates that the main capacitance of Si electrode is regarded to be the pseudocapacitance produced by the ionic diffusion process. Moreover, the value of CPE2 for Si/C electrode is higher compared to Si electrode, which reveals higher electrochemical property for Si/C electrode.

4. Conclusion

Si/C nanocomposite is successfully synthesized by dispersing Si nanoparticles in a gel of phenolic resin followed by a subsequent pyrolysis process. The amorphous nature of pyrolyzed carbon in the Si/C nanocomposite is revealed by XRD patterns and Raman analyses. The weight ratio between the Si and C in the prepared nanocomposite is estimated using TG profiles. FE-SEM and TEM studies on the Si/C nanocomposite elucidate the uniform coating of carbon on the Si particles when the weight ratio of the carbon is 58%. As a promising anode material for lithium-ion batteries, the Si/C nanocomposite exhibits an initial reversible capacity of 904 mAh g^{-1} and a high retention of 75% after 50 cycles at a current density of 100 mA g^{-1}. The highly enhanced electrochemical performance of Si/C nanocomposite maybe attributed to the carbon in the composite and the carbon layers on the surface of Si particles, which suppress the volume change of Si upon cycling, prevent the pulverization of the electrode, and increase the electrical conductivity of nanocomposite.

Acknowledgements

This work was supported by the 973 project (2013CB934001), NSF of China (51172024), Fundamental Research Funds for the Central Universities of China (FRF-TP-09-007A).

References

[1] J. Yamaura, Y. Ozaki, A. Morita, A. Ohta, J. Power Sources 43 (1993) 233.
[2] J.R. Szczech, S. Jin, Energy Environ. Sci. 4 (2011) 56.
[3] H. Li, Z.X. Wang, L.Q. Chen, X.J. Huang, Adv. Mater. 21 (2009) 4593.
[4] U. Kasavajjula, C. Wang, A.J. Appleby, J. Power Sources 163 (2007) 1003.
[5] M. Holzapfel, H. Buqa, L.J. Hardwick, M. Hahn, A. Würsig, W. Scheifele, P. Novák, R. Kötz, C. Veit, F.-M. Petrat, Electrochim. Acta 52 (2006) 973.
[6] M.T. McDowell, S.W. Lee, I. Ryu, H. Wu, W.D. Nix, J.W. Choi, Y. Cui, Nano Lett. 11 (2011) 4018.
[7] H. Kim, M. Seo, M.-H. Park, J. Cho, Angew. Chem. Int. Ed. 49 (2010) 2146.
[8] H.C. Tao, L.Z. Fan, X.H. Qu, Electrochim. Acta 71 (2012) 194.
[9] C.K. Chan, R.N. Patel, M.J. O'Connell, B.A. Korgel, Y. Cui, Nano Lett. 4 (2010) 1443.
[10] H. Ma, F. Cheng, J.Y. Chen, J.Z. Zhao, C.S. Li, Z.L. Tao, J. Liang, Adv. Mater. 19 (2007) 4067.
[11] N. Dimov, S. Kugino, M. Yoshio, Electrochim. Acta 48 (2003) 1579.
[12] C.Y. Du, M. Chen, L. Wang, G.P. Yin, J. Mater. Chem. 21 (2011) 15692.
[13] Y.H. Xu, G.P. Yin, Y.L. Ma, P.J. Zuo, X.Q. Cheng, J. Mater. Chem. 20 (2010) 3216.
[14] Z.S. Wen, D. Lu, J.P. Lei, Y.Q. Fu, L. Wang, J.C. Sun, J. Electrochem. Soc. 158 (2011) A809.
[15] Z.P. Guo, E. Milin, J.Z. Wang, J. Chen, H.K. Liu, J. Electrochem. Soc. 152 (2005) A2211.
[16] L.F. Cui, Y. Yang, C.M. Hsu, Y. Cui, Nano Lett. 9 (2009) 3370.
[17] H.C. Tao, L.Z. Fan, Y.F. Mei, X.H. Qu, Electrochem. Commun. 13 (2011) 1332.
[18] Y.S. Wu, Y.H. Lee, Y.L. Tsai, J. Mater. Process. Technol. 208 (2008) 35.
[19] I.S. Kim, G.E. Blomgren, P.N. Kumta, J. Power Sources 130 (2004) 275.
[20] Z.P. Guo, Z.W. Zhao, H.K. Liu, S.X. Dou, J. Power Sources 146 (2005) 190.
[21] I. Kovalenko, B. Zdyrko, A. Magasinski, B. Hertzberg, Z. Milicev, R. Burtovyy, I. Luzinov, G. Yushin, Science 334 (2011) 75.
[22] J.S. Bridel, T. Azais, M. Morcrette, J.M. Tarascon, D. Larcher, Chem. Mater. 22 (2009) 1229.
[23] K.A. Trick, T.E. Saliba, Carbon 33 (1995) 1509.
[24] Y. Liu, J.S. Xue, T. Zheng, J.R. Dahn, Carbon 34 (1996) 193.
[25] M.S. Wang, L.Z. Fan, M. Huang, J. Li, X. Qu, J. Power Sources 219 (2012) 29.
[26] C. Meier, S. Lüttjohann, V.G. Kravets, H. Nienhaus, A. Lorke, H. Wiggers, Phys. E: Low-dimensional Syst. Nanostructu. 32 (2006) 155.
[27] C. Kim, S.H. Park, J.I. Cho, D.Y. Lee, T.J. Park, W.J. Lee, K.S. Yang, J. Raman Spectrosc. 35 (2004) 928.
[28] H. Li, X.J. Huang, L.Q. Chen, G.W. Zhou, Z. Zhang, D.P. Yu, Y.M.J.M. Yu, N. Pei, Solid State Ionics 135 (2000) 181.
[29] X.D. Wu, Z.X. Wang, L.Q. Chen, X.J. Huang, Electrochem. Commun. 5 (2003) 935.
[30] T. Jiang, S.C. Zhang, X.P. Qiu, W.T. Zhu, L.Q. Chen, Electrochem. Commun. 9 (2007) 930.
[31] C.Y. Du, C.H. Gao, G.P. Yin, M. Chen, L. Wang, Energy Environ. Sci. 4 (2011) 1037.
[32] J. Graetz, C.C. Ahn, R. Yazami, B. Fultz, Electrochem. Solid-State Lett. 6 (2003) A194.
[33] C.K. Chan, H. Peng, G. Liu, K. McIlwrath, X.F. Zhang, R.A. Huggins, Y. Cui, Nat. Nano 3 (2008) 31.
[34] S.H. Ng, J. Wang, D. Wexler, S.Y. Chew, H.K. Liu, J. Phys. Chem. C 111 (2007) 11131.
[35] Y.S. Hu, R. Demir-Cakan, M.-M. Titirici, J.-O. Müller, R. Schlögl, M. Antonietti, J. Maier, Angew. Chem. Int. Ed. 47 (2008) 1645.
[36] J.C. Guo, X.L. Chen, C.S. Wang, J. Mater. Chem. 20 (2010) 5035.
[37] R. Ruffo, S.S. Hong, C.K. Chan, R.A. Huggins, Y. Cui, J. Phys. Chem. C 113 (2009) 11390.